# Effect of streamwise cross-sectional variation on liquid retention in liquid-infused substrates under an external flow

L. Mazor
*Faculty of Aerospace Engineering, Technion Israel Institute of Technology, Haifa 32000, Israel*

H. A. Stone
*Department of Mechanical and Aerospace Engineering, Princeton University, Princeton, New Jersey 08544, USA*

I. Jacobi*
*Faculty of Aerospace Engineering, Technion Israel Institute of Technology, Haifa 32000, Israel*

(Received 21 January 2019; published 23 July 2019)

Lubricant infused in micropatterned substrates will drain in the presence of an external, immiscible shear flow, but this drainage can be retarded by using the substrate geometry to exploit capillary effects at the interface. Recent work [Wexler *et al.*, Phys. Rev. Lett. **114**, 168301 (2015)] produced general geometric guidelines for the design of substrates to oppose this shear drainage in rectangular grooves with uniform cross section in the streamwise direction of the external flow. In this study, we generalize the fluid-retention predictions for lubricant-infused grooves with slowly varying cross section and interfacial geometries. Accounting for interfacial deformation is found to reduce the predicted lubricant retention in geometrically uniform grooves, albeit differently from past predictions. Streamwise nonuniformity in groove cross section is shown to provide little benefit to lubricant retention but may potentially cause significant reductions in retention, and thus should be considered carefully when establishing substrate manufacturing tolerances. An optimal groove shape for maximal lubricant-retention length is derived, although its practical use appears limited by its small surface area coverage compared to uniform grooves.

DOI: 10.1103/PhysRevFluids.4.074003

## I. BACKGROUND

Recent interest in microstructured, liquid-infused substrates has focused on their potential use for creating omniphobic, protective surface coatings [1–3] or drag-reducing surfaces [4–7]. In these applications, a substrate is covered in open capillary grooves that are filled with an omniphobic lubricant immiscible with respect to the external fluid of the operating environment. This creates a substrate that is effectively coated in the trapped lubricant, in much the way traditional superhydrophobic surfaces create a substrate covered with a plastron of air. However, unlike air-infused superhydrophobic surfaces, the non-negligible viscosity of infused lubricant means that the groove is susceptible to lubricant loss by external shear flow. Previous studies were performed to determine the basic capillary groove design criteria necessary for maintaining the infused lubricant even in the presence of such shear flows by balancing the capillary pressure gradient induced by lubricant drainage against the shear stress causing the drainage [8–11]. However, these studies

*ijacobi@technion.ac.il

 

TABLE I. The relevant scales for the lubrication analysis.

| Variable | Scale | Definition | Description |
|---|---|---|---|
| $y$ | $\ell$ | $\ell \sim h$ | Depth of groove |
| $z$ | $\ell$ | $\ell \sim a$ | Half width of groove |
| $x$ | $L$ | $L \sim \ell/\sqrt{\mathrm{Ca}}$ | Length of groove |
| $p$ | $\Pi$ | $\Pi \sim \gamma/\ell$ | Capillary pressure |
| $u$ | $U$ | $U \sim \frac{\ell\lvert\tau_{\mathrm{ext}}\rvert}{\mu_o}$ | Streamwise velocity |
| $v$ | $V$ | $V \sim U\frac{\ell}{L}$ | Vertical velocity |
| $w$ | $W$ | $W \sim U\frac{\ell}{L}$ | Spanwise velocity |

employed *ad hoc*, one-dimensional models to describe the lubricant behavior inside rectangular cross-section, longitudinally uniform, capillary grooves.

The behavior in longitudinally uniform but nonrectangular-cross-sectional open capillaries has previously been studied in the context of imbibition and drainage and, in particular, the time dependence of these processes. Numerical studies of the drainage in a V-shaped groove, later generalized to other cross sections, showed that the traditional Washburn time variation of the location of the wetting front was maintained [12,13]. The nonrectangular-cross-sectional geometries considered in these studies have since been extended to problems of drag reduction in liquid-infused capillary surfaces [14,15]. But in all cases, the streamwise (longitudinal) uniformity of the cross-sectional profile has been assumed.

Longitudinally nonuniform capillaries have also been the subject of interest in problems of imbibition and drainage, with studies of closed capillaries [16] and porous media [17] and even optimal capillary shape variations to maximize capillary rise behavior [18]. Similarly, it has long been recognized that nonuniform spacing of the side walls of open-capillary structures can be used for passive fluid transport by exploiting the differential surface curvature on opposite ends of fluid slugs [19–22].

Because longitudinal variation in surface curvature has such a profound effect on liquid slug transport, the question arises of whether such variation could affect the fluid retention in lubricant-infused open capillaries subject to an external shear flow. The previous experimental analysis of such grooves neglected streamwise variations in groove cross section, and thus the current theoretical study introduces small streamwise variations in both groove and interfacial geometry in order to examine their influences on the steady-state lubricant retention under external shear flow.

### A. Groove drainage geometry

Consider a rectilinear groove initially filled with lubricant, oriented longitudinally in the same direction as a two-dimensional, mean external shear flow. The effect of an external, immiscible shear flow on the flow within such grooves has received significant treatment in recent years, with particular attention drawn to the dependence of the interfacial shear stress on the viscosity ratio between the inner and outer fluids [23,24] and the deformation of the interface between the fluids [25]. These effects on the interfacial shear stress tend to be small compared to the effect of changing groove geometry under consideration in the current study, particularly for narrow or deep grooves (see Appendix A), and thus the interfacial shear stress is assumed equal to the constant external shear stress, $\tau_{\mathrm{ext}} < 0$. The groove depth, $h(x)$, and half-width, $a(x)$, are assumed to both be of magnitude $\ell$ (see Table I) and can both vary with streamwise position, $x$, measured from the downstream terminus of the groove, as illustrated in the top of Fig. 1. The streamwise length scale has magnitude $L$. The external fluid and infused lubricant have interfacial tension, $\gamma$, and density difference $\Delta\rho$. The lubricant has dynamic viscosity $\mu_o$. If we define the capillary length scale, $\lambda_c$, in terms of gravitational acceleration, $g$, as $\lambda_c = \sqrt{\gamma/(g\Delta\rho)}$ and Bond number, $\mathrm{Bo} = (a/\lambda_c)^2$, then for $\mathrm{Bo} \ll 1$

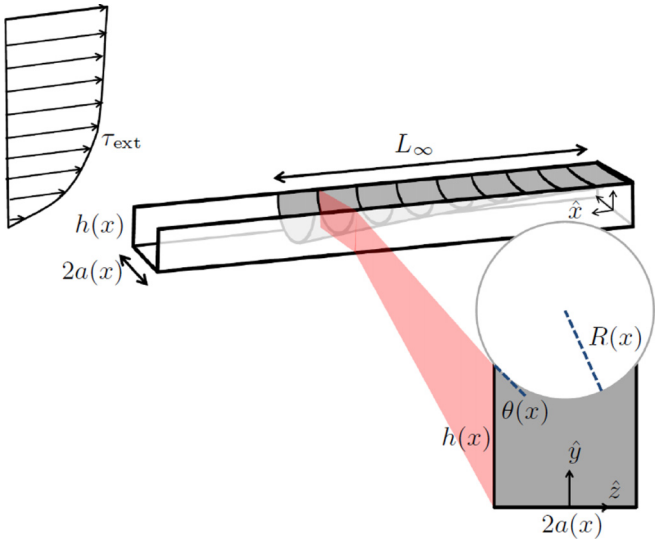


FIG. 1. The geometry of a rectangular domain, showing (top) the isometric overview with steady-state retention length of lubricant, $L_\infty$, and a single cross section highlighted; and (bottom) a cross-sectional view, showing the radius of curvature, $R(x)$, contact angle, $\theta(x)$, and groove half width $a(x)$ and depth $h(x)$. The interface and oil in the groove are colored gray. The external, two-dimensional flow profile is illustrated with its associated shear stress, $\tau_{\text{ext}}$.

we assume that the interfacial shape between the two fluids in any cross section of the groove can be approximated as nearly circular, with radius of curvature $R(x)$ (Appendix D). Under this assumption, the local contact angle at the upper corner of the groove, $\theta(x)$, is then geometrically constrained by the remaining geometric parameters according to

$$R(x) = \frac{a(x)}{\cos[\theta(x)]}. \tag{1}$$

As a result of the external flow, lubricant will drain from the groove in the downstream direction, $-\hat{x}$, until internal pressure gradients in the lubricant balance the external shear, and a length of fluid $L_\infty$ remains. At steady state, the upstream contact angle where the drainage has occurred (at $x = L_\infty$) is assumed to equal the receding contact angle, $\theta_r$. The receding contact angle is defined in the cross-sectional plane, transverse to the direction of drainage, but is assumed to be a relevant proxy for the relevant upstream condition in the actual three-dimensional flow, based on previous experimental observations [8]. For consistency with previous analysis, the groove is assumed to terminate (at $x = 0$) in a fluid reservoir, and thus the downstream angle is assumed to equal $\pi/2$ for a flat interface. Finite grooves without a reservoir were already shown to produce a reservoir-like condition as they overflow at the downstream end, producing large, persistent, reservoir-like droplets on the substrate surface [11].

In the previous modeling of the steady-state fluid retention for a uniform rectilinear groove [8], the variation in interfacial shape, $R(x)$ was neglected. Instead, the interface was assumed to be flat [$R(x < L_\infty) = \infty$] everywhere except for the upstream edge of the infused fluid, $x = L_\infty$, where the curvature $R_r$ was fixed by the receding contact angle, as illustrated in Fig. 2.

The local interfacial curvature can be related to the local pressure drop across the interface via the Young-Laplace equation. Assuming the external flow has no pressure gradient (pressure is $p_w$ everywhere outside the lubricant), the interfacial curvature dictates the local pressure within the

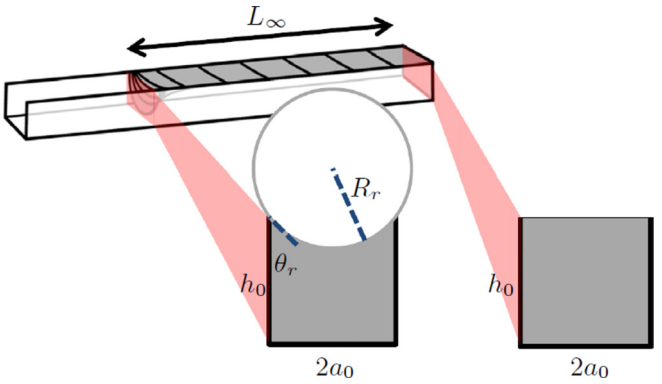


FIG. 2. The steady-state geometry of a uniform rectangular grid, corresponding to the calculations performed in Wexler *et al.* [8], showing (top) the isometric overview with steady-state length of lubricant, $L_\infty$, and the upstream and downstream cross sections highlighted, with all interfacial curvature confined to the upstream end; and (bottom) the cross-sectional views, showing the upstream radius of curvature, $R_r$, receding contact angle, $\theta_r$, and groove half width $a_0$ and depth $h_0$. The interface and lubricant in the groove is colored gray.

lubricant, according to

$$p(x) = p_w - \frac{\gamma}{R(x)}. \tag{2}$$

By nondimensionalizing all of the flow variables with capillary scales according to Table I and using the previous approximation that the interface is flat everywhere except the leading edge, the streamwise pressure gradient within the lubricant can be approximated:

$$\frac{\partial p}{\partial x} \approx \frac{\Delta p}{L_\infty} = -\frac{1}{R_r L_\infty} < 0. \tag{3}$$

In other words, the difference in interfacial curvature over the length of the lubricant induces a favorable pressure gradient in the upstream direction, opposing the direction of the external shear flow, $\tau_{\text{ext}} < 0$. This establishes a competition between a downstream, shear-driven flow and an upstream, pressure-driven flow within the lubricant. The mass balance for these respective flows can be used to define the retention length, $L_\infty$. In order to obtain this mass balance, we must develop the equations governing the flow in the lubricant, under the assumption that the longitudinal extent of the groove, $L$, is much larger than the characteristic dimension of the cross section, $\ell$, i.e., the lubrication approximation.

### B. Lubrication approximation in the groove

The capillary number for the lubricant phase can be written in terms of the interfacial shear or the internal velocity gradient within the lubricant phase, with $U$ as a characteristic velocity scale, yielding

$$\text{Ca} \equiv \frac{\mu_o U}{\gamma} \equiv \frac{\ell|\tau_{\text{ext}}|}{\gamma} \equiv \left(\frac{\ell}{L}\right)^2. \tag{4}$$

Therefore, the assumption that longitudinal variations in the groove are much smaller than cross-sectional variations is identical to the assumption that $\text{Ca} \ll 1$. The Reynolds number for the lubricant flow is defined as $\text{Re} = \frac{\rho U \ell}{\mu_o}$. Writing the three-dimensional momentum equations in

nondimensional form, using the capillary and Reynolds number definitions, and enforcing the lubrication approximation yields

$$\left(\frac{\partial^2}{\partial z^2}+\frac{\partial^2}{\partial y^2}\right)u(y,z)=\frac{\partial p}{\partial x}+O(\mathrm{Re}\sqrt{\mathrm{Ca}}), \tag{5a}$$

$$0=\frac{\partial p}{\partial y}+O(\mathrm{Ca}), \tag{5b}$$

$$0=\frac{\partial p}{\partial z}+O(\mathrm{Ca}), \tag{5c}$$

and thus lubrication analysis follows from the independent assumptions that $\mathrm{Ca}\ll 1$ and $\mathrm{Re}\sqrt{\mathrm{Ca}}\ll 1$.

In order to solve the Poisson-type lubrication equation for the streamwise velocity, $u(y,z)$, the cross-sectional domain of the lubricant must be specified. The location of the circular interface, $y=\eta(x,z)$, can be written in terms of the contact angle and groove aspect ratio, $a/h$, as

$$\frac{\eta(x,z)}{h(x)}=1+\frac{a(x)}{h(x)}\tan[\theta(x)]-\frac{a(x)}{h(x)}\sqrt{\sec^2[\theta(x)]-\frac{z^2}{a(x)^2}}. \tag{6}$$

Then, the no-slip and matched-shear (or tangential stress) boundary conditions on the walls and interface can be written as

$$u|_{y=0}=0,\quad u|_{z=\pm a}=0,\quad \left.\frac{\partial u}{\partial y}\right|_{y=\eta(x,z)}=-1. \tag{7}$$

Because of the lubrication approximation, the pressure gradient in the lubricant can be assumed locally constant, i.e., it develops slowly in $x$, and thus the velocity $u(y,z)$ can be solved as a function of that locally constant pressure gradient $\frac{dp}{dx}$. The solution, $u(y,z)$, can also be linearly decomposed into a shear-driven contribution, $u_s(y,z)$, and a pressure-driven contribution, $u_p(y,z)$, where $u(y,z)=u_\mathrm{s}(y,z)+u_\mathrm{p}(y,z)$, and these components can then be integrated over the cross-sectional area (in the $y$-$z$ plane) to obtain the volumetric flow rates, $q_s$ and $q_p$, according to

$$q_s=\int_{-a}^{a}\int_{0}^{\eta(x,z)}u_s(y,z)\,dy\,dz,\quad q_p=\int_{-a}^{a}\int_{0}^{\eta(x,z)}u_p(y,z)\,dy\,dz. \tag{8}$$

The volumetric flow rates depend only on the cross-sectional geometry of the groove and thus can expressed in terms of positive geometrical functions of the cross-sectional aspect ratio $a(x)/h(x)$, $c_s(a/h)$, and $c_p(a/h)$, to obtain

$$q_s(x)=-c_s a h^2<0,\quad q_p(x)=-c_p a h^3\frac{dp}{dx}>0 \tag{9}$$

for any cross-sectional location, $x$.

At steady state, the mass balance at a single cross section dictates

$$q_s+q_p=0, \tag{10}$$

which yields the constraint that

$$-\frac{dp(x)}{dx}=\frac{1}{h(x)}\frac{c_s(a(x)/h(x))}{c_p(a(x)/h(x))}. \tag{11}$$

This constraint provides the tool needed to obtain the steady-state retention length, $L_\infty$. The left-hand side represents the slow global variation in the pressure gradient, which is locally constant to

satisfy the lubrication assumption. The right-hand side represents the volumetric flow through any given cross section of the lubricant, assuming a locally constant pressure gradient.

In our previous analysis [8], the pressure gradient was assumed globally constant (3) and the cross section of the lubricant was assumed rectangular and constant, as illustrated above. For a rectangular cross section, the coefficient functions $c_p$ and $c_s$ can be expressed as $c_{p,0}$ and $c_{s,0}$ from the solution of the momentum equation (see next section). Substituting the constant pressure gradient then yields

$$L_{\infty,0} \approx \cos(\theta_r)\frac{h_0}{a_0}\frac{c_{p,0}}{c_{s,0}}, \tag{12}$$

which is just the nondimensionalized form of the lubricant retention predicted previously.

In the current study, we consider two generalizations to this analysis: The interfacial deformation is included and therefore the cross section of lubricant is not rectangular [thus changing the right-hand side of Eq. (11)]; and the pressure gradient is assumed to vary slowly with $x$ as a result of interfacial and groove geometry [thus changing the left-hand side of Eq. (11)].

In Sec. II, we consider different techniques for representing the effect of the nonrectangular domain, and we develop an expression for the varying pressure gradient as a function of groove geometry, in order to rewrite the mass balance (11) in generalized form. In Sec. III, the generalized mass balance is solved for the case of a uniform groove and results are compared with the previous theoretical analysis. Finally, Sec. IV considers the effects of streamwise-varying width and depth on the retention length of lubricant.

## II. GENERALIZED MASS BALANCE

### A. Nonrectangular cross section

In order to account for the nonrectangular-cross-sectional domain of the lubricant with a curved interface, we solve the momentum equation by the method of domain perturbation, perturbing the flat interface by a small amount to reflect the interfacial curvature. Introducing the complement to the contact angle, $\varepsilon = \pi/2 - \theta(x)$, which is small for a nearly flat interface, we can approximate the interface location, $\eta(z, x)$, given in Eq. (13), as

$$\eta(x, z) \approx h(x) + \frac{[z^2 - a(x)^2]}{2a(x)}\varepsilon + O(\varepsilon^3), \tag{13}$$

and then seek a solution of the streamwise velocity in the form $u(y, z) = u_0(y, z) + \varepsilon\, u_1(y, z) + \cdots$. As before, this solution can be decomposed into shear- and pressure-driven components. Solving the governing equations (5) and (7) by Fourier series at each order of $\varepsilon$ yields velocity components:

$$u_{s,0}(y, z) = -a\sum_{n=0}^{\infty} B_n \cos(k_n z)\sinh(k_n y), \quad k_n = \frac{\pi}{2a}(2n+1), \tag{14a}$$

$$u_{s,1}(y, z) = -a\sum_{m=0}^{\infty} C_m \cos(k_m z)\sinh(k_m y), \tag{14b}$$

$$u_{p,0}(y, z) = -\frac{dp}{dx}h^2\sum_{n=0}^{\infty}\sum_{m=0}^{\infty} F_{nm}\cos(k_n z)\sin(\ell_m y), \quad \ell_m = \frac{\pi}{2h}(2m+1), \tag{14c}$$

$$u_{p,1}(y, z) = -\frac{dp}{dx}h^2\sum_{j=0}^{\infty} G_j \cos(k_j z)\sinh(k_j y), \tag{14d}$$

where the Fourier series coefficients are given by

$$B_n = \frac{8(-1)^n}{\cosh(k_n h)\pi^2(2n+1)^2}, \tag{15a}$$

$$C_m = \sum_{n=0}^{\infty} \begin{cases} -\frac{B_n}{2\pi}\frac{\sinh(k_n h)}{\cosh(k_m h)}\frac{(-1)^{n+m}(1+2n)^3}{(n-m)^2(1+n+m)^2}, & m \neq n, \\ B_n \tanh(k_m h)\frac{3+\pi^2(1+2m)^2}{6\pi(1+2m)}, & m = n, \end{cases} \tag{15b}$$

$$F_{nm} = \frac{64}{\pi^4}\frac{(-1)^n}{(2m+1)(2n+1)\left[\frac{h^2}{a^2}(2n+1)^2+(2m+1)^2\right]}, \tag{15c}$$

$$G_j = \frac{a^2}{h^2}\sum_{n=0}^{\infty} \begin{cases} \sum_{m=0}^{\infty} F_{nm}\frac{\sin(\ell_m h)}{\cosh(k_j h)}\frac{(-1)^{n+j}(1+2n)(1+2m)^2}{2\pi(n-j)^2(1+n+j)^2}, & j \neq n, \\ -\sum_{m=0}^{\infty} F_{nm}\frac{\sin(\ell_m h)}{\cosh(k_j h)}\frac{[3+\pi^2(1+2j)^2](2m+1)^2}{6\pi(1+2j)^3}, & j = n. \end{cases} \tag{15d}$$

The volumetric flow rates over the cross section (8) can be represented in the form of factors $c_s$ and $c_p$ (9), which can also be written at each order of $\varepsilon$ as

$$c_s = c_{s,0} + \varepsilon\, c_{s,1} + \cdots, \quad c_p = c_{p,0} + \varepsilon\, c_{p,1} + \cdots, \tag{16}$$

where $c_{s,0}$ and $c_{p,0}$ represent the parameters for the flat interface, as above. Substituting the velocities into the volumetric integrals (8) and separating the $y$-integral limits $[0, \eta(x,z)]$ into the sum of $[0,h]$ and $[h, h+\varepsilon(\frac{z^2-a^2}{2a})]$ according to the definition of the interface location (13) yields

$$q_0 + \varepsilon q_1 = \int_{-a}^{a}\left\{\int_0^h u_0(y,z)+\varepsilon u_1(y,z)\,dy + \int_h^{\varepsilon(\frac{z^2-a^2}{2a})} u_0(y,z)+\varepsilon u_1(y,z)\,dy\right\}dz \tag{17a}$$

$$= \int_{-a}^{a}\int_0^h u_0(y,z)\,dy\,dz + \varepsilon\int_{-a}^{a}\left\{\int_0^h u_1(y,z)\,dy\,dz + u_0(h,z)\left(\frac{z^2-a^2}{2a}\right)dz\right\} + O(\varepsilon^2), \tag{17b}$$

where the left Riemann sum has been used to approximate the integrals of width $\varepsilon$. Then, neglecting terms of $O(\varepsilon^2)$ and using the relations between the flowrates and the geometric coefficients (9), we obtain

$$c_{s,0} = \sum_{n=0}^{\infty}\left(\frac{a}{h}\right)^2 B_n \frac{16(-1)^n \sinh^2\left[\frac{\pi h}{4a}(1+2n)\right]}{\pi^2(1+2n)^2}, \tag{18a}$$

$$c_{s,1} = \sum_{m=0}^{\infty} 16(-1)^m\left(\frac{a}{h}\right)^2\left\{\frac{C_m(1+2m)\pi\sinh^2\left[\frac{h\pi}{4a}(1+2m)\right] - B_m \sinh\left[\frac{h\pi}{2a}(1+2m)\right]}{\pi^3(1+2m)^3}\right\}, \tag{18b}$$

$$c_{p,0} = \sum_{n=0}^{\infty}\sum_{m=0}^{\infty} F_{nm}\frac{8(-1)^n}{\pi^2(1+2m)(1+2n)}, \tag{18c}$$

$$c_{p,1} = 16\left(\frac{a}{h}\right)\left\{\sum_{n=0}^{\infty}\sum_{m=0}^{\infty} F_{nm}\frac{(-1)^{1+m+n}}{\pi^3(1+2n)^3} + \sum_{j=0}^{\infty} G_j \frac{(-1)^j \sinh^2\left[\frac{h\pi}{4a}(1+2j)\right]}{\pi^2(1+2j)^2}\right\}, \tag{18d}$$

where $c_{p,0}, c_{s,0} > 0$, whereas $c_{p,1}, c_{s,1} \leqslant 0$ for all $a/h$ and $\theta$. Therefore, the effect of the deformed interface is always to decrease the magnitude of the two opposed volumetric flow rates at any given cross section of the lubricant, which is consistent with the reduced slip length at the interface observed in a recent perturbation analysis of gas-infused hydrophobic surfaces with meniscus curvature [25].

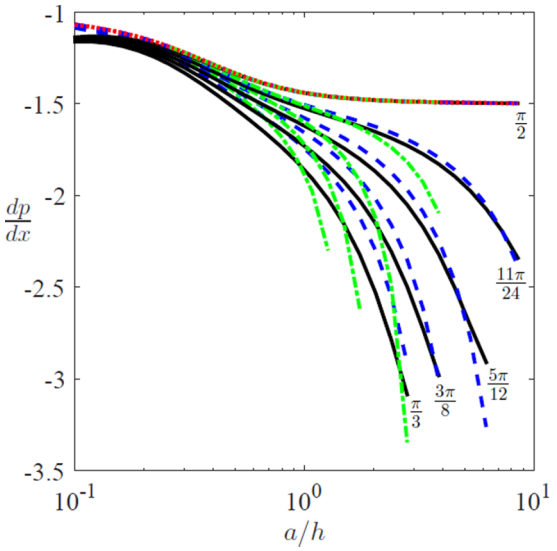


FIG. 3. The steady-state pressure gradient as a function of aspect ratio, $a/h$, and contact angle, $\theta$, calculated numerically over the exact domain (black solid lines); by domain perturbation (green dash-dotted); for a flat interface (red dotted); and using the heuristic scaling of Eq. (20) (blue dashed).

The accuracy of this domain perturbation approximation can be assessed by comparison with a numerical solution of the cross-sectional flow over the exact domain. The numerical solution can be obtained by transforming the actual domain to a rectangle via change of coordinates and solving the resulting transformed equation by Chebyshev collocation [26] as detailed in Appendix B. This numerical procedure can be iterated for any combination of parameters $(a, h, \theta)$ describing the deformed domain of lubricant. At steady state, the net volumetric flow through the domain must be zero, and thus the steady-state value of the pressure gradient, $\frac{dp}{dx}$, which satisfies this no net flow criterion can be found as a function of $(a, h, \theta)$ by iteration. Then, the steady-state pressure gradient found numerically can be compared with the pressure gradient approximated from the $c_s$ and $c_p$ values obtained by domain perturbation (16) as shown in Fig. 3 (green dash-dotted lines). As the groove becomes wider and the constant shear acts on a shallower depth of lubricant, the magnitude of the pressure gradient needed to balance the shear increases.

The original analysis assuming a flat interface fails to capture the significant difference in the pressure gradient as a function of contact angle and aspect ratio (Fig. 3). The domain perturbation solution qualitatively captures these dependencies, particularly for small aspect ratios, $a/h < 1$, where even smaller contact angles result in a minimal reduction in the fluid domain. However, as the aspect ratio becomes larger, even contact angles very near $\pi/2$ can result in significant reductions of the fluid domain area. Thus, even though $\varepsilon$ is small in these cases, the domain perturbation itself is not small in terms of the cross-sectional area change. This means the complement to the contact angle, $\varepsilon$, is not an appropriate perturbation variable since contact angle alone does not adequately capture the reduction in lubricant area.

A better approach for approximating the effect of the deformed interface on $c_s$ and $c_p$ must take into account this reduced area. Heuristically, we can describe the effect of the deformed interface as resulting in a decreased "effective depth" of the groove, $h_{\text{eff}}$, which can be calculated by averaging the interface position across the width of the groove,

$$h_{\text{eff}} \approx \frac{1}{2a}\int_{-a}^{a}\left(h + \frac{z^2 - a^2}{2a}\varepsilon\right)dx = h - \frac{a}{3}\left(\frac{\pi}{2} - \theta\right). \tag{19}$$

Because the volumetric flow rate of shear-driven flow in a groove scales with $h^2$ and pressure-driven flow with $h^3$ as shown in Eq. (9), we can simply rescale the leading-order volumetric flow coefficients by the effective depth to the appropriate power,

$$c_s \approx c_{s,0}\left(\frac{h_{\text{eff}}}{h}\right)^2, \quad c_p \approx c_{p,0}\left(\frac{h_{\text{eff}}}{h}\right)^3. \tag{20}$$

This simple approach has the virtue of correcting for the deformed interface even when the groove is very wide, since it explicitly compensates for the effect of groove aspect ratio. The heuristic approximation can also be used to predict the steady pressure gradient, as shown in Fig. 3 (blue dashed lines) and performs significantly better than the formal, domain perturbation approach. Thus, the heuristic approach is adopted for the remainder of the analysis.

### B. Nonconstant pressure gradient

Besides taking into account the effect of the interface shape locally, at a specific $x$ location, the slow streamwise variation of the interface and groove geometry can also be introduced through the pressure gradient itself on the left-hand side of Eq. (11). In the previous analysis described above, this pressure gradient was assumed globally constant for a flat interface and was defined by the receding contact angle alone. More generally, it can be derived from the Young-Laplace equation using Eqs. (1) and (2) above and differentiating in $x$ to obtain

$$\frac{dp(x)}{dx} = \frac{1}{a(x)^2}\left[\cos(\theta(x))\frac{da(x)}{dx} + a(x)\sin(\theta(x))\frac{d\theta(x)}{dx}\right], \tag{21}$$

where the pressure gradient now varies as a function of groove geometry, $a(x)$, as well as interface geometry, $\theta(x)$.

Substituting the Young-Laplace expression for the pressure gradient and the heuristic approximation for $c_s$ and $c_p$ into the steady-state balance (11) yields

$$-\left[\frac{\left(\frac{c_{s,0}}{c_{p,0}}\right)\left(\frac{a}{h}\right)}{1-\frac{1}{3}\left(\frac{a}{h}\right)\left(\frac{\pi}{2}-\theta\right)}\right] \approx \frac{\cos(\theta)}{a}\frac{da}{dx} + \sin(\theta)\frac{d\theta}{dx}. \tag{22}$$

Thus, we obtain a differential equation that determines the contact angle, $\theta(x)$, at steady state, as a function of the groove geometry, $a(x)$ and $h(x)$. This $\theta(x)$ effectively determines the streamwise variation of the radius of curvature of the channel (Fig. 1). The boundary conditions for $\theta(x)$ are $\theta(x=0) = \pi/2$ for the downstream reservoir and $\theta(x=L_\infty) = \theta_r$ for the upstream receding contact angle. Therefore, given a particular groove geometry, the equation for $\theta(x)$ can be integrated to obtain the steady fluid retention length, $L_\infty$, which enters through the boundary conditions.

## III. UNIFORM GROOVES

For the case of a uniform, rectangular groove considered previously, $a(x) = a_0$ and $h(x) = h_0$, the steady-state balance simplifies to

$$-\left[\frac{\left(\frac{c_{s,0}}{c_{p,0}}\right)\left(\frac{a_0}{h_0}\right)}{1-\frac{1}{3}\left(\frac{a_0}{h_0}\right)\left(\frac{\pi}{2}-\theta\right)}\right] \approx \sin(\theta)\frac{d\theta}{dx}. \tag{23}$$

This equation can be integrated over $x$ from $\theta(x=0) = \pi/2$ to obtain the implicit solution for $\theta(x)$

$$\frac{[6h_0 - a_0\pi + 2a_0\theta(x)]\cos(\theta(x))}{2a_0\sin(\theta(x)) + 6a_0\frac{c_{s,0}}{c_{p,0}}x - 2a_0} \approx 1, \tag{24}$$

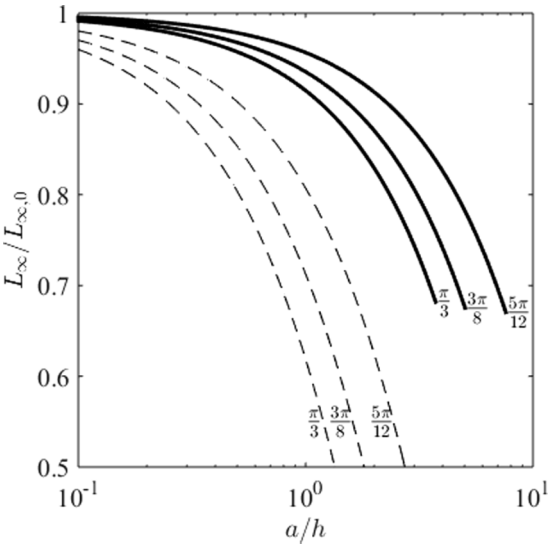


FIG. 4. The steady-state retention length correction factor for a uniform groove, determined by integrating the steady momentum equation (solid black) or approximating the variation of the maximum deformation according to Liu *et al.* [27] (dashed line).

and then solved for the retention length $L_\infty$ at $\theta(x = L_\infty) = \theta_r$ to obtain

$$\frac{L_\infty}{L_{\infty,0}} \approx 1 - \frac{1}{3}\frac{a_0}{h_0}\left[\frac{\pi}{2} - \theta_r + \tan(\theta_r) - \sec(\theta_r)\right], \tag{25}$$

where $L_{\infty,0}$ represents the retention length for a entirely flat interface (12). Therefore, the effect of interfacial deformation is to reduce the fluid retention length in the groove compared to the case of an assumed flat interface.

A similar correction for the effect of the nonconstant pressure gradient had previously been reported by Liu *et al.* [27] (in their Appendix C, defined in terms of variable $\chi$), where they assumed a linear streamwise variation in the maximum deformation amplitude of the interface. These two corrections to the steady retention length are compared in Fig. 4.

It is apparent that both correction factors for the interfacial deformation indicate a significant reduction in lubricant retention compared to the flat interface prediction, but the current correction factor shows that the effect is less severe (at most 25%) than the previous estimate (50%). The discrepancy between the two correction factors is due the previous assumption that the maximum interfacial deformation varies linearly with $x$; the nonlinear variation predicted in the current study is within 10% of the linear variation (and thus consistent with experimental observations, within measurement error), but that a small difference in the interface shape manifests itself as a significant effect on retention.

## IV. GROOVES WITH VARYING CROSS-SECTION

The slowly varying pressure gradient (21) depends on both the contact angle, $\theta(x)$, examined in the previous section, and the half-width of the groove, $a(x)$. We now consider a groove with a linearly varying half-width, which means integrating Eq. (22) between the two boundary values of $\theta$ to determine the distance between them, $L_\infty$. This means that the domain of integration, in $x$, will vary for each groove geometry.

In order to maintain a fixed domain size, for computational convenience, we recast Eq. (22) over a fixed domain via a coordinate transformation. Let the new streamwise coordinate $s = x/L_\infty$, with

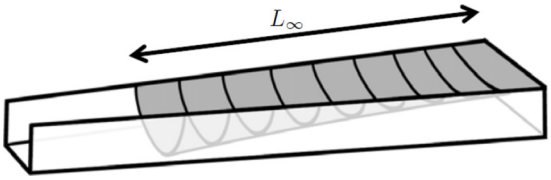


FIG. 5. A trapezoidally shaped groove, with linearly varying half-width, $a(x)$.

a new contact angle $\hat{\theta}(s) = \theta(s L_\infty)$. Similarly, the depth $\hat{h}(s) = h(s L_\infty)$ and half-width $\hat{a}(s) = a(s L_\infty)$. The transformed equation then becomes

$$-L_\infty \left[ \frac{\left(\frac{c_{s,0}}{c_{p,0}}\right)\left(\frac{\hat{a}}{\hat{h}}\right)}{1 - \frac{1}{3}\left(\frac{\hat{a}}{\hat{h}}\right)\left(\frac{\pi}{2} - \hat{\theta}\right)} \right] = \frac{\cos(\hat{\theta})}{\hat{a}} \frac{d\hat{a}}{ds} + \sin(\hat{\theta}) \frac{d\hat{\theta}}{ds}, \tag{26}$$

which is evaluated over the fixed domain $s \in [0, 1]$, with the same boundary conditions $\hat{\theta}(0) = \theta_0$, $\hat{\theta}(1) = \theta_r$, but now explicitly containing the unknown parameter, $L_\infty$, which can be solved easily using MATLAB's "bvp4c" finite-difference solver.

If we assume that the half-width varies linearly with groove extent, starting from $a_0$ at the downstream terminus, according to

$$\hat{a}(s) = a_0 + a' s, \quad a' \in (-a_0, a_{\max} - a_0), \tag{27}$$

we obtain a trapezoidal groove shape illustrated in Fig. 5. The maximum width of a groove, before the occurrence of dewetting of the lubricant along the groove floor, is $a_{\max} < h(x)(\sec(\theta) + \tan(\theta))$. The slope of the half-width, $a'$, is thus constrained to produce grooves with nonzero width everywhere while also avoiding dewetting.

In order to evaluate the effect of the trapezoidal grooves on lubricant retention, the lubricant retention length $L_\infty^{\text{linear}}$ for each trapezoidal groove is compared to the retention length of a uniform groove with the identical average half-width, $L_\infty^{\text{uniform}}$, as illustrated in Fig. 6. Grooves that widen in the streamwise direction $a' > 0$ result in significant reductions in fluid retention, by as much as 15%. In this case, the pressure gradient contributed by the widening groove opposes the capillary pressure gradient generated by the interfacial variation. On the other hand, grooves that narrow in the streamwise direction, $a' < 0$, result in only modest increases in retention length, less than 2%. However, for the widening grooves, the assumption of constant interfacial stress can no longer be justified as the fluid depth in the groove center decreases (see Appendix A) and thus we are unable to make definitive claims about the magnitude of the reduction in retention for those cases, beyond a qualitative note of caution.

The groove depth, $h(x)$ also contributes to the balance between shear- and pressure-driven flows (22) and thus we consider the effect of linear variation in groove depth, according to

$$\hat{h}(s) = h_0 + h' s, \quad h' \in [h_{\min} - h_0, \mathcal{O}(1)], \tag{28}$$

where the mininum depth to avoid dewetting is $h_{\min} > \sec(\theta) - \tan(\theta)$, and there is no limit on the maximum depth, except that the quantities must remain consistent with the lubrication assumptions. As before, the lubricant retention length $L_\infty^{\text{linear}}$ for each groove of linearly varying depth is compared to the retention length of a uniform groove with the identical average depth, $L_\infty^{\text{uniform}}$, as illustrated in Fig. 7.

Linearly varying groove depth nearly always reduces the retention length because the capillary pressure gradient remains unchanged but the shear-driven flow rate is effectively increased over some finite length of groove compared to the uniform groove. The effect of varying groove depth is strongest for very shallow grooves or grooves that become very shallow over some distance. However, as noted above, the assumption of uniform external shear at the interface cannot be justified for shallow grooves, in which the variations in interfacial shear may be at least as important

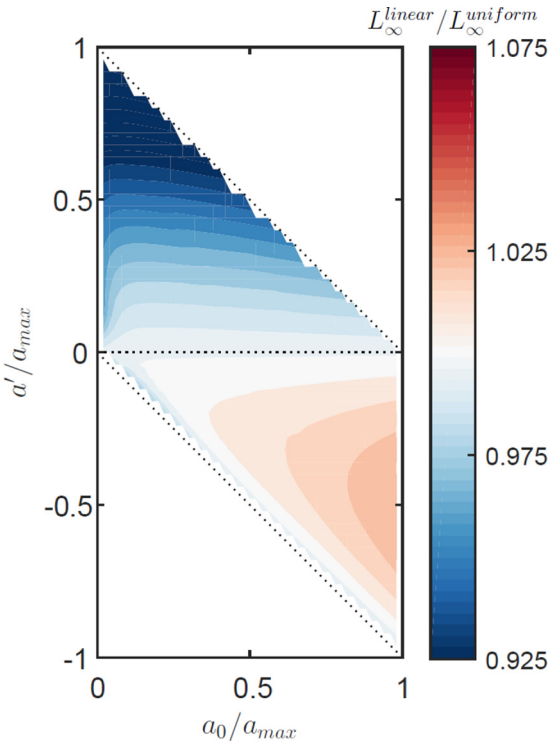


FIG. 6. The ratio of retained fluid in a groove with linearly varying half-width, $L_\infty^{\text{linear}}$, vs a uniform groove of the same average aspect ratio, $L_\infty^{\text{uniform}}$, as a function of downstream width, $a_0$, and wall slope, $a'$. Calculations were performed for $\theta_r = \pi/3$.

as the variations in groove geometry, as explained in Appendix A. Thus, we cannot draw any definite conclusions about the effect of depth variation using the current analytical framework, although the magnitude of the effect could potentially be quite large and thus may serve as a warning for the manufacturing of capillary grooves on nonuniform substrates, where depth may vary.

### A. Optimal shape for maximal retention length

According to the mechanism observed in previous experiments (and assumed here), the region of lubricant retention extends until the contact angle at the upstream end of the groove reaches the receding contact angle. Thus, preventing drainage from the groove would require an interface shape in which the contact angle never reaches the receding contact angle. One way to enforce this condition is to require no variation in the contact angle at all, $\frac{d\theta}{dx} = 0$. In this case, the governing equation (22) can be simplified to obtain an equation for the groove shape slope $\frac{da}{dx}$ needed to balance the shear flow but without contact angle variation:

$$-\left[\frac{\left(\frac{c_{s,0}}{c_{p,0}}\right)\left(\frac{a}{h_0}\right)}{1-\frac{1}{3}\left(\frac{a}{h_0}\right)\left(\frac{\pi}{2}-\theta\right)}\right] \approx \frac{\cos(\theta)}{a}\frac{da}{dx}. \tag{29}$$

This differential equation can be solved numerically to obtain an optimal groove shape, $a(x)$, that is predicted to retain an infinite length of fluid, for fixed groove depth, $h_0$. Of course for the equation to be well defined, $\theta \neq \pi/2$ and the surface cannot be completely flat; the curvature must be able to vary with the changing aspect ratio in order to produce the pressure gradient to oppose the shear.

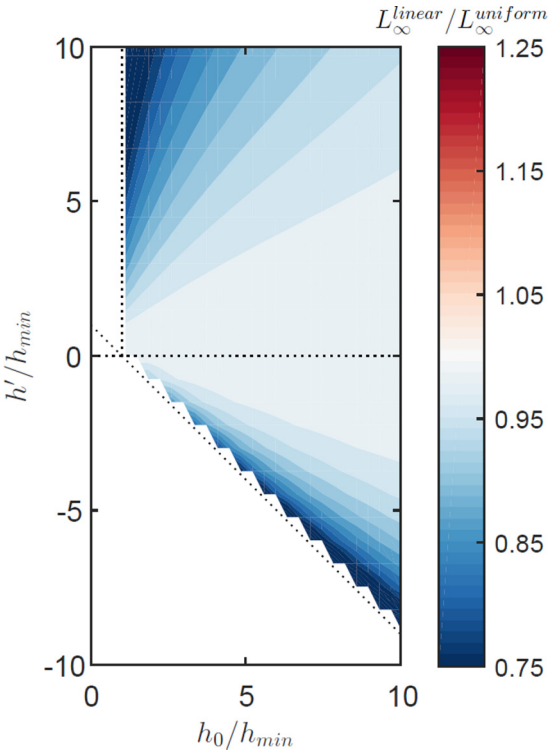


FIG. 7. The ratio of retained fluid in a groove with linearly varying depth, $L_\infty^{\text{linear}}$, vs a uniform groove of the same average aspect ratio, $L_\infty^{\text{uniform}}$, as a function of downstream depth, $h_0$, and floor slope, $h'$. Calculations were performed for $\theta_r = \pi/3$.

Because the optimal shape predicted would, in principle, produce an infinitely long extent of fluid, with a half-width that approaches 0, some numerical cutoff on the minimum width, $a_{\text{min}} = 0.01\, a_0$, must be selected in order to define a practical retention length, $L_\infty^{\text{eff}}$. In practice, this minimum width might be the result of manufacturing limitations. The effective retention length can then be compared to a uniform groove with identical average half-width. Despite the practical cutoff, the optimal groove still retains roughly an order of magnitude longer length of fluid than a uniform groove, over all initial aspect ratios: $L_\infty^{\text{eff}}/L_\infty^{\text{uniform}} = O(10)$.

However, the optimal shape has a half-width that varies as $a(x) \sim x^{-1}$ (Appendix C) and thus the total surface area coverage of these grooves, over some practical finite length (until $a_{\text{min}}$ is reached), is negligible compared to uniform grooves, and they would seem to serve little useful purpose. However, the basic idea of a sharply narrowing groove that can maintain a uniform contact angle in the contained lubricant may find applications in the design of the leading edge of uniform grooves. Instead of an abrupt, rectangular terminus, the uniform groove could begin with an optimally shaped narrow region to suppress the initiation of drainage.

## V. CONCLUSIONS

As liquid-infused substrates become more widely used for manufacturing robust and drag-reducing surfaces, more detailed analysis of their ability to retain infused fluid becomes crucial. In this study, the original analysis of Wexler *et al.* [8] was generalized to include the effects of interfacial deformation, and these effects were represented in a simple model and compared with numerical solutions to the lubrication flow problem. The effect of interfacial deformation on lubricant retention

was found to differ from previous predictions by a factor of nearly two. The model was then applied to the problem of streamwise, linearly varying groove geometries, and it was shown that in most cases, the optimal retention can be accomplished with simple uniform grooves, but that certain types of streamwise nonuniformity may potentially be detrimental to lubricant retention. Finally, an optimal groove shape for maximizing longitudinal liquid retention was developed, although its practical applications may be quite limited due to its small surface area coverage.

## ACKNOWLEDGMENTS

This research was supported by Grant No. 2014208 from the United States–Israel Binational Science Foundation (BSF). The authors thank Prof. Beni Cukurel for the helpful suggestion regarding depth-varying grooves and an anonymous referee for insights on the constant external stress assumption.

## APPENDIX A: CONSTANT INTERFACIAL STRESS ASSUMPTION

We assume that shear stress of the external flow, $\tau_{\text{ext}}$, applies uniformly along the fluid-fluid interface of the groove. Strictly speaking, however, the shear stress along the groove interface, $\tau_s(x, z)$, is not uniform or identical to the outer stress; rather, it differs due to the different viscosities of the two immiscible fluids and the nonflat shape of the interface. The question is whether the discrepancy between the external shear stress and the actual interfacial shear stress is significant when compared to the magnitude of the geometric variations under consideration. If the actual interfacial shear stress varies weakly with respect to changes in groove geometry, then we can justify the assumption that the interfacial shear stress is constant as we study geometric affects on fluid retention. In order to answer this question, we treat the two causes for shear stress variation separately. First, assuming that the fluid interface remains flat, the variation in interfacial shear stress with changing groove cross section can be calculated explicitly from the results of Schönecker and Hardt [23]. The interfacial shear stress, $\tau_s$, for the shear flow with viscosity ratio between the lubricant and external fluid, $\lambda = \mu_o/\mu_{\text{ext}}$, maximum local slip length $d$ at the interface, and normalized slip length, $D_\ell = d/(2a)$, is given by

$$\tau_s = \frac{1}{1 + 2D_\ell \lambda^{-1}}, \tag{A1}$$

where the shear stress is written nondimensionally (in terms of the applied external shear, $\tau_{\text{ext}}$). This result is identical to the experimentally validated result of Liu *et al.* [27] [Eq. (9a)]. The expression for the normalized slip length is given in Schönecker and Hardt [23] [Eq. (2.16)],

$$D_\ell = d_{0,\ell}\text{erf}\left(\frac{\sqrt{\pi}}{4d_{0,\ell}}\frac{h}{a}\right), \tag{A2}$$

where $d_{0,\ell} \approx 0.347$ is calculated numerically, for a single groove. Thus, we can calculate the dependence of the shear stress for a flat groove on the half-width of the groove, $a$, and groove height, $h$, as

$$\frac{d\tau_s}{da} = \frac{\lambda^{-1}\left(\frac{h}{a}\right)\exp\left[-\left(\frac{h}{a}\frac{\sqrt{\pi}}{4d_{0,\ell}}\right)^2\right]}{a\left[1 + 2d_{0,\ell}\lambda^{-1}\text{erf}\left(\frac{h}{a}\frac{\sqrt{\pi}}{4d_{0,\ell}}\right)\right]^2}, \tag{A3}$$

$$\frac{d\tau_s}{dh} = \frac{-\lambda^{-1}\exp\left[-\left(\frac{h}{a}\frac{\sqrt{\pi}}{4d_{0,\ell}}\right)^2\right]}{a\left[1 + 2d_{0,\ell}\lambda^{-1}\text{erf}\left(\frac{h}{a}\frac{\sqrt{\pi}}{4d_{0,\ell}}\right)\right]^2}. \tag{A4}$$

The results for the full range of possible groove aspect ratios, $h/a$, are plotted in Fig. 8 in the black, solid lines. We see that, at least for a flat interface, the effect of the shear stress variation

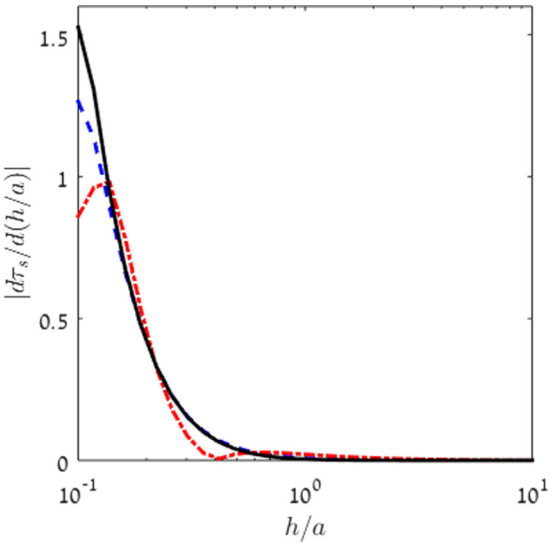


FIG. 8. The nondimensionalized variation of interfacial shear stress for a flat interface at the centerline, $\tau_s(z = 0, y = \eta)$, with respect to variations the aspect ratio of the groove, $h/a$ for $\lambda = 2$. Theory from Schönecker and Hardt [23] in solid black line; numerical calculations of the theory for flat interface in blue dashed line; numerics for curved interface in red dash-dotted line.

is negligible compared to the effect of the variation in aspect ratio, $h/a$, for $h/a \gtrsim 0.3$. This result is robust over a wide range of viscosity ratios. So, if we are studying the effect of variations in $a$ or $h$ for narrower or deeper grooves, it is reasonable to assume that $\tau_s$ is roughly constant, and we can employ $\tau_{\text{ext}}$ as its proxy. However, the shear stress varies more strongly with aspect ratio for shallower and wider grooves and more care must be taken. But this analysis does not yet consider the effect of the deformed interface on the groove fluid behavior, as studied via perturbation methods by Crowdy [25]. To check the effect of the interface shape, even for larger contact angles beyond that considered with perturbation analysis, we extended the numerical solution of the flow, described in Appendix B, to include both lower and upper phases, with stress and velocity matching conditions between them. In the upper phase, far from the interface, the shear stress was fixed at $\tau_{\text{ext}}$, and the two phases were solved as a pair of coupled Poisson problems, iteratively. In this formulation, the groove corners (triple-point lines) are singular and must be removed numerically, but the solution trends were validated against the theory, at least for the flat interface, providing confidence in the simplistic approach. Using the numerical solution, the graphs of the interfacial stress variation with groove cross section were calculated again, this time taking into account the curved interface, shown in the red dash-dotted lines in Fig. 8. The trends were found to be roughly the same. Therefore, the discrepancy between the local interfacial stress and the external shear stress, due to groove interfacial shape or viscosity mismatch, is considered small when compared to the effects of cross-sectional geometry variation for sufficiently deep (narrow) grooves, and is neglected in those cases. For shallow (wide) grooves, the varying interfacial shear stress cannot be necessarily be neglected.

## APPENDIX B: NUMERICAL SOLUTION

To solve the governing lubrication flow equation with inhomogeneous boundary conditions over the deformed cross-sectional domain, we stretch the deformed domain in the $y$ direction, to "flatten" the curved interface, by defining a new coordinate system:

$$(z', y') = \left[\frac{z}{a}, \frac{y}{\eta(z)}\right]. \tag{B1}$$

Then, the governing equation is transformed (and the new unit normal for the now flat interface is $\mathbf{n}' = (0, -1, 0)$ since $\frac{\partial \eta'}{\partial z'} = 0$ in the new coordinate system):

$$\left[\frac{\partial^2}{\partial z'^2} + \left(\frac{a}{\eta(z')}\right)^2 \frac{\partial^2}{\partial y'^2}\right] u(y', z') = a^2 \frac{\partial p}{\partial x} \tag{B2}$$

with boundary conditions

$$u|_{y'=0} = 0, \quad u|_{z'=\pm 1} = 0, \quad \left.\frac{\partial u}{\partial y'}\right|_{y'=1} = -\eta(z'). \tag{B3}$$

Spectral collocation is used to solve this PDE in the transformed coordinates (using the Chebyshev collocation packages developed by Trefethen [26]) and then transform it back into physical coordinates. The resulting velocity field can be integrated to obtain the volumetric flow rate as a function of the flow and geometrical parameters.

## APPENDIX C: APPROXIMATE OPTIMAL GROOVE SHAPE

A close approximation to the numerical solution for the optimal groove shape can be obtained assuming that the groove depth is fixed, $h_0$, that the ratio $\frac{c_{s,0}}{c_{p,0}}$ is a constant, defined by $a_0/h_0$, and that the interfacial shape deformation is negligible (contrary to the earlier analysis) with fixed contact angle $\theta_0$. This yields

$$-\left(\frac{c_{s,0}}{c_{p,0}}\right)\left(\frac{a}{h}\right) \approx \frac{\cos(\theta_0)}{a}\frac{da}{dx}, \tag{C1}$$

which can be integrated easily to obtain

$$\frac{a(x)}{a_0} \approx \left(1 + \frac{a_0}{h_0}\frac{c_{s,0}}{c_{p,0}}\frac{x}{\cos(\theta_0)}\right)^{-1}. \tag{C2}$$

The approximate solution is asymptotically similar to the numerical solution (with relative error $<50\%$) and thus serves as a useful analytical representation for optimal groove design.

## APPENDIX D: WIDE GROOVES AND GRAVITY

The fluid retention analysis throughout the current study assumed that the interface shape was roughly circular, based on the assumption that the relevant length scale of the groove, $a$, is smaller than the capillary length scale, $\lambda_c = \sqrt{\gamma/(\Delta\rho g)}$ (written dimensionally). Because previous experimental studies always considered microscopic grooves in liquid-liquid systems, this condition was easily satisfied.

As the groove becomes much wider, close to or exceeding the capillary length scale, the interface shape can flatten due to gravitational effects. Therefore, even in the uniform groove case, the effective radius of curvature at the receding (upstream) end of the groove (i.e., the radius of curvature evaluated prior to dewetting) will be larger than that predicted by a circular geometric fit, and the induced capillary pressure gradient will be less, thus resulting in less fluid retention. This situation is analogous to the problem of the meniscus shape for capillary rise in an arbitrarily sized tube, first solved numerically by Adams and Bashforth [28] and later expressed in a more convenient, parametric form [29].

Taking gravity into account, the effective radius of curvature, $R_{\text{eff}}$, can be written as an asymptotic series in Bond number, in terms of the circular-sector radius of curvature, $R$, used above, and coefficient $\alpha$ that depends on contact angle:

$$R_{\text{eff}} \approx [1 + \alpha(\theta)\,\text{Bo}]R, \tag{D1}$$

where for small Bond number the coefficient function is given by [29]

$$\alpha(\theta) = \tfrac{1}{6}\sec(\theta)[3\sec(\theta) - 2\sec^3(\theta) + 2\tan^3(\theta)]. \tag{D2}$$

This asymptotic approximation is accurate to within <2% (compared to the exact numerical solution) even up to Bond numbers of 2, over a wide range of contact angles (25–75°). The contact angle dependence is quite weak, and thus replacing $\alpha(\theta)$ by the average value of $\alpha$ over all possible angles, $\overline{\alpha} = 0.14$, produces a model still accurate to within 2.5%.

The original derivation of the steady-state fluid retention balance can then be rederived with a streamwise, Bond number dependence, $\mathrm{Bo}(x)$, using $R_{\mathrm{eff}}$ and employing $\overline{\alpha}$ for simplicity, where

$$\frac{dp}{dx} = \frac{(1 + 3\overline{\alpha}\,\mathrm{Bo})\cos(\theta)\frac{da}{dx} + (1 + \overline{\alpha}\,\mathrm{Bo})a\sin(\theta)\frac{d\theta}{dx}}{(1 + \overline{\alpha}\,\mathrm{Bo})^2 a^2}. \tag{D3}$$

In the case of a uniform groove with $a$ and $h$ constant, the steady retention decreases as the Bond number (groove width) increases. For a Bond number at the upper end of the asymptotic range, $\mathrm{Bo} \approx 2$, the reduction in fluid retention can exceed 20%, which is a non-negligible effect. This correction factor is useful in practical engineering problems where microscopic grooves may be difficult to produce on a substrate, and specifically where the density of the outer fluid is very small in comparison to the infused liquid, thus inflating the Bond number. For gas flow over a liquid, the Bond number is easily an order of magnitude larger, in which case the interfacial distortion becomes prominent.


[1] T.-S. Wong, S. H. Kang, S. K. Y. Tang, E. J. Smythe, B. D. Hatton, A. Grinthal, and J. Aizenberg, Bioinspired self-repairing slippery surfaces with pressure-stable omniphobicity, Nature (London) **477**, 443 (2011).

[2] A. Lafuma and D. Quéré, Slippery pre-suffused surfaces, Eur. Phys. Lett. **96** 56001 (2011).

[3] J. D. Smith, R. Dhiman, S. Anand, E. Reza-Garduno, R. E. Cohen, G. H. McKinley, and K. K. Varanasi, Droplet mobility on lubricant-impregnated surfaces, Soft Matter **9**, 1772 (2013).

[4] B. R. Solomon, K. S. Khalil, and K. K. Varanasi, Drag reduction using lubricant-impregnated surfaces in viscous laminar flow, Langmuir **30**, 10970 (2014).

[5] C. Lee, C. H. Choi, and C. J. Kim, Superhydrophobic drag reduction in laminar flows: A critical review, Exp. Fluids **57**, 1 (2016).

[6] B. J. Rosenberg, T. Van Buren, M. K. Fu, and A. J. Smits, Turbulent drag reduction over air- and liquid-impregnated surfaces, Phys. Fluids **28**, 015103 (2016).

[7] H. Chen, Y. Gao, H. A. Stone, and J. Li, "Fluid bearing" effect of enclosed liquids in grooves on drag reduction in microchannels, Phys. Rev. Fluids **1**, 083904 (2016).

[8] J. S. Wexler, I. Jacobi, and H. A. Stone, Shear-Driven Failure of Liquid-Infused Surfaces, Phys. Rev. Lett. **114**, 168301 (2015).

[9] I. Jacobi, J. S. Wexler, M. A. Samaha, J. K. Shang, B. J. Rosenberg, M. Hultmark, and H. A. Stone, Stratified thin-film flow in a rheometer, Phys. Fluids **27**, 052102 (2015).

[10] J. S. Wexler, A. Grosskopf, M. Chow, Y. Fan, I. Jacobi, and H. A. Stone, Robust liquid-infused surfaces through patterned wettability, Soft Matter **11**, 5023 (2015).

[11] I. Jacobi, J. S. Wexler, and H. A. Stone, Overflow cascades in liquid-infused substrates, Phys. Fluids **27**, 082101 (2015).

[12] R. R. Rye, J. A. Mann, and F. G. Yost, The flow of liquids in surface grooves, Langmuir **12**, 555 (1996).

[13] L. A. Romero and F. G. Yost, Flow in an open channel capillary, J. Fluid Mech. **322**, 109 (1996).

[14] A. A. Hemeda and H. Vahedi Tafreshi, Instantaneous slip length in superhydrophobic microchannels having grooves with curved or dissimilar walls, Phys. Fluids **27**, 102101 (2015).

[15] P. Dey, S. K. Saha, and S. Chakraborty, Microgroove geometry dictates slippery hydrodynamics on superhydrophobic substrates, Phys. Fluids **30**, 122007 (2018).

[16] M. Reyssat, L. Courbin, E. Reyssat, and H. A. Stone, Imbibition in geometries with axial variations, J. Fluid Mech. **615**, 335 (2008).
[17] D. Shou, L. Ye, J. Fan, K. Fu, M. Mei, H. Wang, and Q. Chen, Geometry-induced asymmetric capillary flow, Langmuir **30**, 5448 (2014).
[18] B. Figliuzzi and C. R. Buie, Rise in optimized capillary channels, J. Fluid Mech. **731**, 142 (2013).
[19] J.-C. Baret, M. Decre, S. Herminghaus, and R. Seemann, Transport dynamics in open microfluidic grooves, Langmuir **23**, 5200 (2007).
[20] J. Berthier and K. A. Brakke, Droplets between two non-parallel planes: From tapered planes to wedges, in *The Physics of Microdroplets* (Scrivener Publishing, Beverly, MA, 2012), pp. 143–160.
[21] J. Feng and J. P. Rothstein, One-way wicking in open micro-channels controlled by channel topography, J. Colloid Interface Sci. **404**, 169 (2013).
[22] A. Ghosh, R. Ganguly, T. M. Schutzius, and C. M. Megaridis, Wettability patterning for high-rate, pumpless fluid transport on open, non-planar microfluidic platforms, Lab Chip **14**, 1538 (2014).
[23] C. Schönecker and S. Hardt, Longitudinal and tranverse flow over a cavity containing a second immiscible fluid, J. Fluid Mech. **717**, 376 (2013).
[24] C. Schönecker, T. Baier, and S. Hardt, Influence of the enclosed fluid on the flow over a microstructured surface in the Cassie state, J. Fluid Mech. **740**, 168 (2014).
[25] D. G. Crowdy, Perturbation analysis of subphase gas and meniscus curvature effects for longitudinal flows over superhydrophobic surfaces, J. Fluid Mech. **822**, 307 (2017).
[26] L. N. Trefethen, *Spectral Methods in MATLAB* (SIAM, Philadelphia, 2000).
[27] Y. Liu, J. S. Wexler, C. Schönecker, and H. A. Stone, Effect of viscosity ratio on the shear-driven failure of liquid-infused surfaces, Phys. Rev. Fluids **1**, 074003 (2016).
[28] F. Bashforth and J. C. Adams, *An Attempt to Test the Theories of Capillary Action by Comparing the Theoretical and Measured Forms of Drops of Fluid* (Cambridge University Press, Cambridge, UK, 1883).
[29] P. Concus, Static menisci in a vertical right circular cylinder, J. Fluid Mech. **34**, 481 (1968).